ACS Sustainable Resource Management

pubs.acs.org/acssrm Article

Residual *Phaeodactylum tricornutum*-Derived Biochar for Effective Removal of Pb(II) from Wastewater

Anjon Kumar Mondal,* Cora Hinkley, C. I. Sathish, Ajayan Vinu, Stalin Kondaveeti, Farjana Akter, Peter Ralph, and Unnikrishnan Kuzhiumparambil*

Cite This: https://doi.org/10.1021/acssusresmgt.5c00556 Read Online

ACCESS | Metrics & More | Article Recommendations | Supporting Information

ABSTRACT: Microalgae offer the potential to generate a range of high-value products, and after the extraction of value-added compounds, the residual biomass can be upcycled to truly turn "waste" into wealth within a zero-waste biorefinery framework. In this study, residual *Phaeodactylum tricornutum* biomass obtained after lipid extraction was utilized to produce biochar via pyrolysis at three different temperatures. The physicochemical properties show that the biochar obtained from 550 °C exhibits a higher amount of inorganic nutrients (K, Mg, Na, Ca, P, Fe), a porous and disordered structure, a moderately higher specific surface area, and active functional groups. When applied as a contaminant adsorbent, the biochar shows significant Pb removal efficiency with a maximum adsorption capacity of 476.19 mg/g. A kinetic and adsorption isotherm study revealed that the adsorption is well-defined by the pseudo-second-order model and the Langmuir adsorption isotherm model, respectively.

KEYWORDS: *Phaeodactylum, residual biomass, biochar, removal efficiency, adsorption, wastewater*

1. INTRODUCTION

In recent years, the quality and availability of potable water have significantly deteriorated due to industrial development and related human activities. The constant release of various pollutants, including inorganic and organic contaminants and heavy metals, into water bodies via industrial wastewater effluents and excess stormwater is the primary reason for water degradation, directly affecting human health and water security. The worldwide annual discharge of untreated industrial wastewater and sewage into water bodies is around 172 billion cubic meters.[1] As of 2022, 2.2 billion people were unable to access safe drinking water, and more than 6 billion people will face the challenge of accessing quality water globally by 2050.[2,3]

Due to its high mobility and persistence, lead (Pb) is considered one of the most toxic heavy metals released into water bodies through industrial effluents.[4] It accrues easily in living organisms even at a very low concentration and causes human health complications, including anemia and high blood pressure, particularly for middle-aged and older people.[5] Long-term contact with Pb causes severe damage to the kidney, nervous system, and brain in adults.[5,6] Moreover, the high Pb concentration causes adverse effects on neurodevelopment, including decreased psychological function and impulsivity and carelessness in children.[7] The maximum acceptable level of Pb in drinkable water is 10 μg/L.[8] However, it is found that the Pb concentration is still higher than the permissible limit in surface water and groundwater.[9] Thus, it is an urgent need to measure and remove the excess amount of toxic Pb from water to protect the community's health.

Several treatment methods have been employed to remove pollutants from wastewater, such as precipitation, ion exchange, reverse osmosis, membrane separation, electrochemical treatment, and evaporation. However, most of these methods are costly and therefore not commercially adopted, particularly when the concentration of pollutants is low in wastewater. These methods also generate waste sludge, which presents another problem for practical application.[10] Recently, adsorption has been considered a promising, inexpensive approach for removing contaminants from wastewater due to its ease of operation, low cost, rapidity, and high efficacy.[11] Many adsorbents have been explored for removing Pb(II) from wastewater, including carbon nanotubes, activated carbon, and agricultural waste materials.[12−14] However, the application of these

Received: October 13, 2025
Revised: May 8, 2026
Accepted: May 11, 2026

adsorbents is limited due to their low efficiency, high cost, and low selectivity.[11]

Biochar is a solid product derived from diverse terrestrial and algal biomasses through thermochemical processes, such as pyrolysis, hydrothermal carbonization, and hydrothermal liquefaction.[15−17] Over the past decades, interest in converting biomass into biochar has surged and continues to grow due to its environmental benefits and sustainability.[18] It has also garnered significant research interest globally due to its potential in addressing some of the critical global challenges, including GHG mitigation, environmental pollution, soil amendment, and long-term carbon storage in the soil.[19] Biochar is widely used for removing heavy metals and inorganic and organic pollutants from wastewater due to the availability of feedstocks and intriguing physicochemical properties, including stability, enriched surface functional groups, high specific surface area, large pore volume, and high adsorption capacity.[20,21] The presence of inorganic nutrients in biochar introduces it as an effective fertilizer and conditioner to improve soil fertility and crop productivity by altering the chemical, physical, and biological properties of the soil.[22] The physicochemical properties of biochar vary depending on biomass materials and preparation conditions.

Recently, the production and utilization of biochar from both macro- and microalgae-based biomass have gained tremendous research attention from the scientific community due to their sustainability and diverse physicochemical properties.[23] The biochar preparation from the residual biomass of microalgae after the extraction of lipid, protein, and fatty acids is a promising sustainable approach, which not only reduces the cost of the overall process but also provides a solution for solid waste management.[24] The lipid extraction process disrupts the cell structure of microalgae, breaking it into small fragments and thus increasing the specific surface area of residual biomass and subsequent biochar. Lipid extraction also reduces the yield, carbon content, and the formation of toxic compounds.[25,26] Compared to biochar obtained from other biomasses, residual microalgae-based biochar may exhibit a better adsorption capacity due to its large surface area, porous structure, high mineral content, and rich surface functional groups.[27] Based on the circular economy, the residual algae-based biochar appears as a sustainable and cost-effective alternative for developing wastewater treatment systems.[28]

In this study, we collected residual *Phaeodactylum tricornutum* biomass after extracting lipids and used pyrolysis to prepare biochar at three different temperatures. Several characterization techniques were employed to investigate the properties of the biomaterials. The current work aims to examine (1) the optimal pyrolysis temperature to achieve a material with better quality in respect of structural properties, including surface area, surface functional groups, inorganic minerals, and thermal stability; (2) the feasibility of using residual microalgae-based biochar for Pb adsorption from contaminated water; and (3) the effect of concentration, contact time, and biochar dose on Pb adsorption.

2. EXPERIMENTAL SECTION

2.1. Preparation of Biochar

The residual biomass of *P. tricornutum* was washed repeatedly with MQ water and dried in a freeze dryer for 48 h. The dried biomass was pulverized into a powder using a grinder and then sieved through a 0.25 mm sieve. 30.0 g of biomass powder was taken in a high-purity rectangular alumina crucible and placed in the middle of a horizontal tube furnace (Lab Tech, model STF1200). The biomass was pyrolyzed with a continuous N_2 flow (3.0 L/min) at a heating rate of 10 °C/min to final temperatures of 450, 550, and 650 °C, respectively, for 2 h. N_2 was passed for at least 20 min before heating began, and the N_2 flow was continued after finishing the pyrolysis time until the temperature reached <100 °C. The material was cooled to ambient temperature and stored in air-tight plastic jars for further analysis. The biochar samples obtained from residual *P. tricornutum* biomass at three different temperatures were named as PB450, PB550, and PB650, respectively.

2.2. Characterization

The surface morphology of *P. tricornutum*-derived biochar samples was examined using scanning electron microscopy (SEM) (Zeiss EVO LS15) coupled with energy-dispersive X-ray spectroscopy (EDS). The surface functional groups were determined using Fourier transform infrared (FTIR) spectroscopy in ATR mode (Nicolet FT-IR 6700) in the wavelength range between 4000 and 400 cm^{-1}. The percentages of C and N, as well as the C/N ratio, were analyzed using a CN analyzer (LECO-400). A pH meter (inoLab pH level 2, Germany) was used to measure the pH; 2 g of biochar was dispersed in 20 mL of MQ water (1 W:10 V) and shaken for 20 min. The elemental composition of the biochar samples and the Pb content before and after adsorption were analyzed using ICP-MS (Agilent Technologies 7700 ICP-MS). The nitrogen adsorption–desorption isotherms experiments were performed using an ASAP 2420 instrument from Micromeritics at 77 K. The samples were degassed at 200 °C for 12 h before the measurements, resulting in a 5% weight loss. The Brunauer–Emmett–Teller (BET) and the Barrett–Joyner–Halenda (BJH) methods were used to calculate the specific surface area, pore size distribution, and pore volume. To determine the crystallinity, X-ray diffraction (XRD) (Bruker D8 DISCOVER) was conducted using the range of 2θ from 10° to 80° with a step speed of 5°/min. The thermal stability of biomass and biochar samples was determined by using thermogravimetric analysis (TGA) (TA Instruments SDT Q600-1255). Samples of biomass and biochars produced at different temperatures (approximately 10.0 mg each) were heated to 700 °C at a heating rate of 10 °C/min under a N_2 atmosphere.

2.3. Adsorption Experiment

To assess the adsorption capacity and efficiency, batch experiments were conducted by varying the initial Pb(II) ion concentration, biochar dose, and contact time. A stock solution for the Pb(II) adsorption experiment was prepared by dissolving 10 g of lead(II) nitrate ($Pb(NO_3)_2$) in 1 L of MQ water, resulting in a concentration of 10 g/L. This stock solution was then used to prepare a range of low (0.2, 0.4, 0.6, 0.8, 1.0, and 2 mg/L) and high (0.05, 0.5, 2.0, 3.0, and 5 g/L) concentration solutions of $Pb(NO_3)_2$. 100 mL of 0.2 mg/L solution was placed in three conical flasks, with each flask containing 100 mL of the same concentration. 500 mg of each biochar sample (PB450, PB550, and PB650) was added to three flasks and shaken in a reciprocating shaker at 150 rpm for 24 h. The solutions were filtered through a 0.20 μm syringe filter. The same method was used to evaluate the adsorption efficiency for each concentration of Pb(II). The Pb(II) stock solution for each concentration and all filtered solutions were diluted by 1% HNO_3 and analyzed by using ICP-MS. To prepare the standard curve, a standard solution of Pb(II) was used. The calibration range was 0–100 ppb, and rhodium (Rh) was used as an internal standard. The calibration curve was calculated using the ratio of the element's count per second (CPS) divided by the CPS of the internal standard (rhodium). The internal standard was prepared simultaneously with the sample, and the calibration standard was combined within a t-piece before introduction to the plasma. The dilution factor for each sample was chosen so that the concentration of the elements fell within the calibration. Five technical replicates were

https://doi.org/10.1021/acssusresmgt.5c00556
ACS Sustain. Resour. Manage. XXXX, XXX, XXX−XXX

run for each sample to analyze adsorbed Pb(II) ions for all adsorption-related experiments in ICP-MS. The initial pH of $Pb(NO_3)_2$ solutions at different concentrations was around 6.6. The pH of Pb(II) solutions was adjusted to 6.0 with hydrochloric acid.

The adsorption capacity and adsorption efficiency of the Pb(II) ion were calculated using the following equations:[29]

$$\text{adsorption capacity } (q_e) = \frac{(C_0 - C_e)V}{m} \quad (1)$$

$$\text{adsorptionefficiency } (\%) = (C_0 - C_e)/C_0 \times 100 \quad (2)$$

In which C_0 is the initial concentration and C_e is the final concentration of non-adsorbed Pb(II), while V (L) is the volume of solution and m (mg) is the weight of the biochar.

2.4. Desorption Experiment

To evaluate the reusability of biochar, adsorption experiments were conducted by using 5 repeated adsorption–desorption cycles. After each adsorption cycle, 25 mL of 0.2 M HCl (desorbing agent) solution was added and shaken for 2 h to regenerate the biochar. After each desorption process, the HCl solution was discarded and washed with MQ water to reuse the biochar. 100 mL of 500 mg/L Pb(II) solution was added after each regeneration process and shaken at 150 rpm for 24 h. After each adsorption–desorption cycle, the lead content was determined by using ICP-MS.

2.5. Adsorption Kinetics

The mathematical formulas of the pseudo-first-order (PFO) and pseudo-second-order (PSO) kinetic models are presented in eqs 3 and 4, respectively.[30]

$$\ln(q_e - q_t) = \ln q_e - k_1 t \quad (3)$$

$$t/q_t = 1/k_2 q_{e2} + t/q_e \quad (4)$$

where q_e is the adsorbed amount (mg/g) of Pb(II) at equilibrium and q_t is the adsorbed amount (mg/g) at time t. k_1 and k_2 are the rate constants of the adsorption of PFO and PSO, respectively.

2.6. Adsorption Isotherm

The linear form of the Langmuir and Freundlich isotherms can be expressed according to eqs 5 and 6:[31]

$$C_e/q_e = 1/K_L q_m + C_e/q_m \quad (5)$$

$$\ln q_e = \ln K_F + 1/n(\ln C_e) \quad (6)$$

in which C_e and q_e are the concentration and adsorption capacity, respectively, at equilibrium, K_L is the Langmuir adsorption constant (L/mg), q_m is the maximum adsorption capacity, and K_F and n are the Freundlich constants related to the adsorption capacity and adsorption intensity, respectively. K_L, K_F, q_m, and n can be calculated from the slope and intercept of the linear fitting C_e/q_e versus C_e.

3. RESULTS AND DISCUSSION

3.1. Properties of Biochar

3.1.1. Surface Morphology. The morphology of residual *P. tricornutum* biomass-derived biochar samples was examined by SEM. Figure 1 shows the low- and high-magnification SEM images of biochar samples prepared at three different pyrolysis temperatures. As shown in Figure 1a–f, all biochar samples display uneven and porous structures. These structures were developed because of the volatilization of organic matter during the pyrolysis.[31]

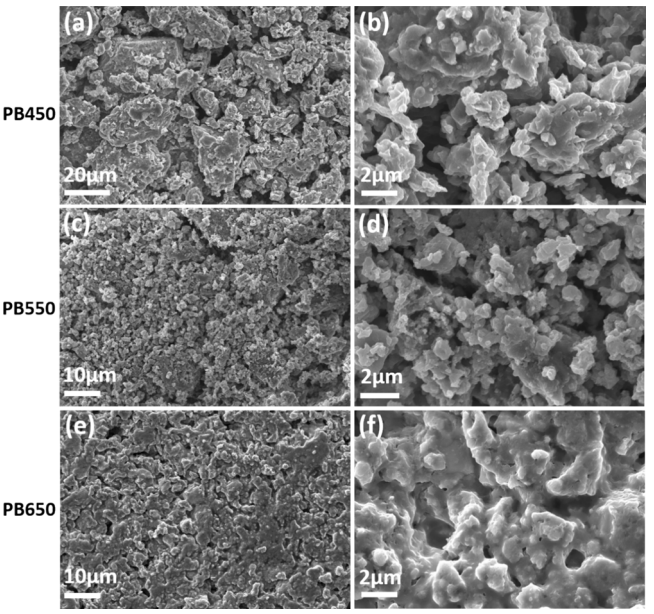

Figure 1. SEM images of *Phaeodactylum* residue-derived biochars. PB450: (a) low magnification and (b) high magnification; PB550: (c) low magnification and (d) high magnification; and PB650: (e) low magnification and (f) high magnification.

However, PB550 shows more damaged and porous structures, cavities, and channels (Figure 1c,d) compared to PB450 (Figure 1a,b) and PB650 (Figure 1e,f). This is due to the release of more volatile matter and the decomposition of more organic substances from etching pores during the pyrolysis at 550 °C. The presence of channels, pores, and cavities on the surface of PB550 biochar could be beneficial for adsorption of Pb.[32]

The nitrogen adsorption–desorption analysis was carried out to study the porosity nature and the textural properties of the biochar. The isotherms and the BJH pore size distribution of biochar samples pyrolyzed at 450, 550, and 650 °C are shown in Figure 2.

All the biochar samples reveal a type IV isotherm with a H3 hysteresis loop (P/P^0 = 0.4–0.9), which is an indication of mesoporous character of the materials.[33] The BET specific surface areas of PB450, PB550, and PB650 were measured to be 6.07, 8.75, and 1.18 m^2/g, respectively. As noticed, by increasing the pyrolysis temperature from 450 to 550 °C, an increase in the surface area could be noticed, which might be due to the degradation of organic matter. Further increasing the temperature to 650 °C, the surface area decreased to 1.18 m^2/g. The BJH pore size distribution results are presented in the insets of Figure 2a–c. The total pore volumes were calculated to be 0.025, 0.047, and 0.004 cm^3/g. The pore size distributions illustrate a narrow distribution, where most of the pores range from 1.8 to 5 nm, further confirming the mesoporous character of the material and the presence of both micro- and mesopores. Generally, the surface area, porosity, and pore volume increase with increasing pyrolysis temperature. However, higher temperatures cause pores and defects to collapse, resulting in a decrease in the surface area and pore volume of biochar.[24] This was also consistent with the SEM

https://doi.org/10.1021/acssusresmgt.5c00556
ACS Sustain. Resour. Manage. XXXX, XXX, XXX–XXX

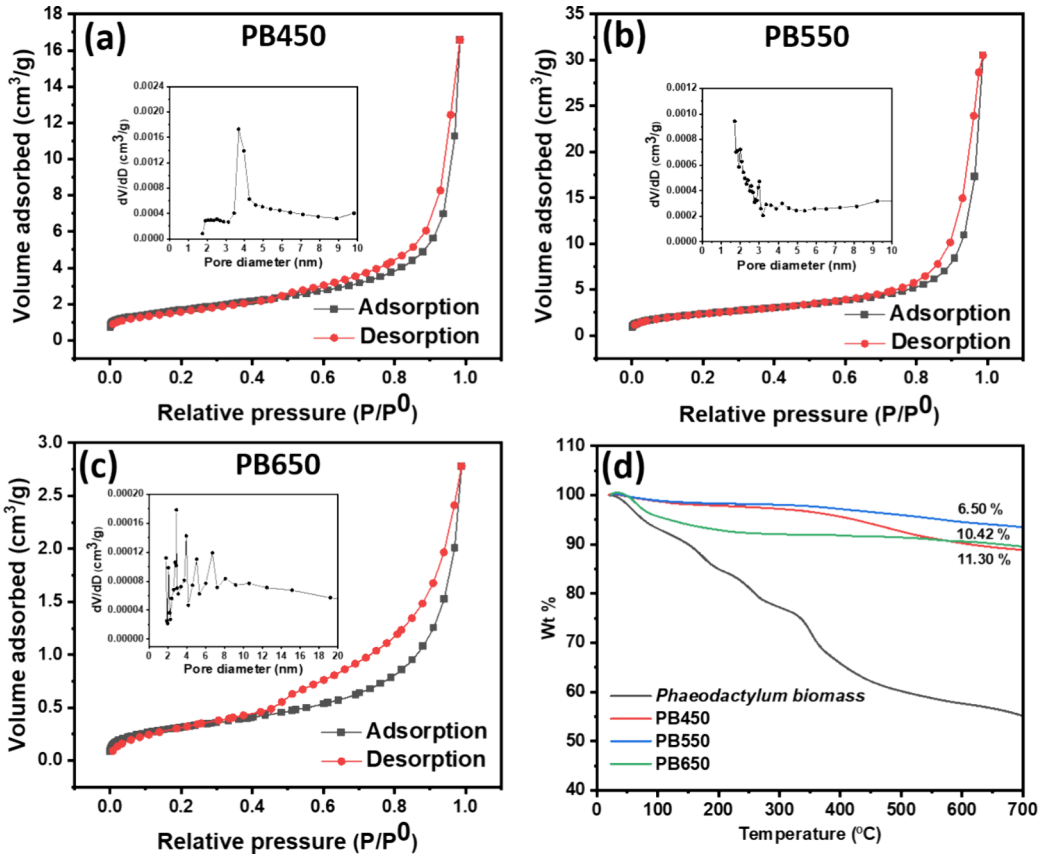

Figure 2. Nitrogen adsorption–desorption isotherms and corresponding BJH pore size distributions (inset) of (a) PB450, (b) PB550, and (c) PB650; (d) TGA curves of *Phaeodactylum* residual biomass and biochar samples at different temperatures.

images of PB650 (Figure 1e,f), where the morphology was quite regular, and few pores were observed. In the current investigation, PB550 shows the highest specific surface area and pore volume compared to PB450 and PB650. Therefore, PB550 biochar may exhibit a greater adsorption capability for Pb than PB450 and PB650.

3.1.2. Thermal Stability. Figure 2d displays the thermogravimetric (TGA) curves of *Phaeodactylum* residual biomass and biochar samples. As shown in Figure 2d, the thermal degradation of biomass can be categorized into three main stages. In the first stage (room temperature to approximately 170 °C), a ∼12% weight loss was observed, which is attributed to the removal of moisture content and highly volatile compounds from the biomass.[34] A major weight loss of 48% was found in the second stage (170–550 °C). The decomposition of organic compounds occurred within this temperature range, and for this reason, this stage is called the active pyrolytic zone or devolatilization stage.[35] In the third stage (550–700 °C), degradation of biomass proceeds slowly and the thermally stable compounds are decomposed, resulting in the formation of biochar.[36] The TGA curves of biochar samples differ from the TGA curve of residual biomass, where weight loss occurs in two steps: a moderate weight loss of up to 600 °C for biochar samples was due to the removal of adsorbed water from the biochars and the second weight loss from 600 to 700 °C represents the decomposition of thermally stable compounds.[37] The TGA curves of the biochar samples show that the total weight loss of PB550 (6.50%) is less than those of PB450 (11.30%) and PB650 (10.42%), indicating that PB550 is more thermally stable than PB450 and PB650.

3.1.3. Elemental Analysis. The physicochemical properties of biochar produced at different temperatures are shown in Table 1. All biochar samples show higher yields, ranging from 67.46 to 72.88%, and high ash content, ranging from 64.21 to 68.66%. The C and N contents of *Phaeodactylum* biomass are 20.33 and 3.55%, respectively.

The C and N contents in PB450, PB550, and PB650 biochar samples are very low, which is due to the extraction of lipids from *P. tricornutum* before the use of residual biomass. The overall quality of biochar in terms of morphology, yield, inorganic minerals, and ash content differs with pyrolysis temperature.[38] The C/N ratio is one of the main parameters for metal adsorption. The higher C/N ratio specifies the biochar, which will be rich in carbohydrates with carboxyl-dominant functional groups.[39] As shown in Table 1, the amount of inorganic minerals (Ca, Na, K, Mg, P, and Fe) is higher in PB550 compared to PB450 and PB650, demonstrating that PB550 could have increased adsorption capacity through cation exchange.[24]

3.1.4. X-ray Diffraction. XRD analysis was conducted to examine the crystallinity and phase purity of *Phaeodactylum* residue-derived biochars prepared at temperatures of 450, 550, and 650 °C. As shown in Figure 3a, a plenty of narrow and sharp diffraction peaks of several mineral phases (K, Na, Mg, P, and Ca) were observed in all biochar samples. Among other peaks, the diffraction peaks appeared at 25.7°, 28.50°, 30.5°, 32.7°, 36.68°, and 40.6° in biochars are attributed to the

https://doi.org/10.1021/acssusresmgt.5c00556
ACS Sustain. Resour. Manage. XXXX, XXX, XXX–XXX

Table 1. Physicochemical Properties of Biochars Obtained from *Phaeodactylum* Residue

parameters	units	PB450	PB550	PB650
yield	%	72.88	71.34	67.46
ash	%	64.208	68.66	66.89
carbon (C)	%	3.36	4.04	1.72
nitrogen (N)	%	0.54	0.55	0.59
C/N ratio		6.22	7.34	2.91
oxygen (O)	%	26.61	19.34	24.55
Ca	g/kg	0.075	0.084	0.080
Na	g/kg	4.30	4.85	4.61
K	g/kg	23.80	27.30	26.23
Mg	g/kg	5.52	6.23	5.84
P	g/kg	0.97	1.11	1.03
Fe	g/kg	0.38	0.43	0.42

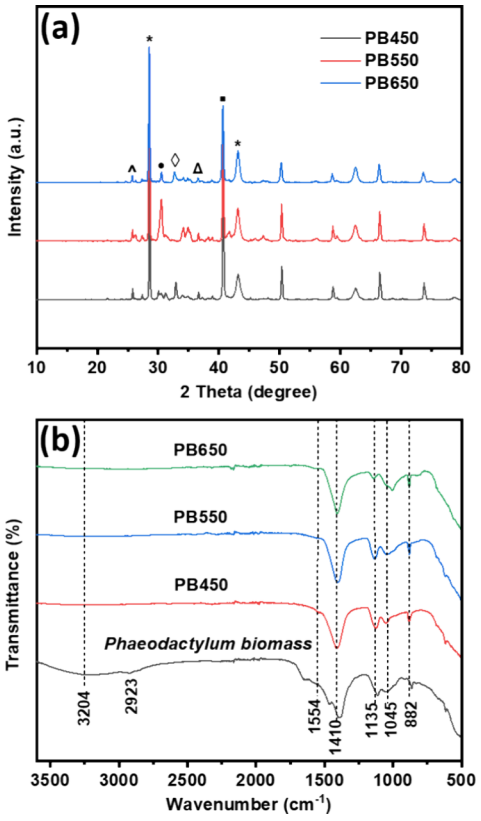

Figure 3. (a) XRD spectra for PB450, PB550, and PB650. ^ represents $MgSO_4$, $K_2MgSi_5O_{12}$, and $Ca_3(PO4)_2$; * represents $CaCO_3$; • represents KCl and K_2SO_4; ◊ represents NaCl; Δ represents $Ca_3Mg_2(PO_4)_4$; • indicates K_2SiO_3. (b) FTIR spectra of *Phaeodactylum* residual biomass and biochars.

presence of different mineral components in the form of $MgSO_4$, $K_2MgSi_5O_{12}$, $Ca_3(PO4)_2$, $CaCO_3$, KCl, NaCl, $Ca_3Mg_2(PO_4)_4$, and K_2SiO_3.[24,40] The peaks within the range of 50–75° are assigned to the silicates and quartz of Ca and Mg.[41] The sharpness and intensity of the diffraction peaks in PB550 were greater than those of the peaks in PB450 and PB650, indicating that more mineralization occurred at a temperature of 550 °C.[42] The elemental analysis and EDS spectra (Table 1 and Figure S1) also confirmed the presence of inorganic minerals in biochar samples. The degree of degradation of organic matter and the progression of mineral components depend on pyrolysis temperature.

3.1.5. Surface Functional Groups. The surface functional groups of *Phaeodactylum* residual biomass and biochars at different temperatures were analyzed using FTIR, and the relevant spectra are presented in Figure 3b. For *Phaeodactylum* residue, a broad band at 3204 cm^{-1} was ascribed to the hydroxyl (–OH) group and the band at 2923 cm^{-1} was related to the –CH stretching of the aliphatic component.[43] After pyrolysis at different temperatures, these two bands almost disappeared and aromatization increased, which is attributed to the decomposition of phenolic and alcoholic functionalities and the elimination of methyl groups from the aromatic rings in biochars.[44] A number of bands at 1554, 1410, 1135, and 1045 cm^{-1} are observed in all biochar samples, which are assigned to the presence of carboxyl functional groups (C=O) on the surface of biochars.[45] The band located at 882 cm^{-1} represents the deformation of aromatic C–H bending. The presence of a C=O group increases the adsorption capacity of metal ions through a complexation mechanism.[46] A higher C/N ratio indicates the presence of a higher quantity of C=O groups in biochar. In this study, the C/N ratio of PB550 is higher (7.34) than those of PB450 (6.22) and PB650 (2.91), which demonstrates the presence of more C=O groups in PB550 (Table 1). Thus, PB550 may have a higher Pb adsorption capacity than PB450 and PB650.

3.2. Adsorption of Pb(II)

3.2.1. Effect of Pyrolysis Temperature. The effect of pyrolysis temperature on the adsorption of Pb was initially investigated using 50 and 500 mg/L Pb(II) solutions. As shown in Figure 4a, at a concentration of 50 mg/L, PB450, PB550, and PB650 demonstrated exceptional removal efficiencies of 99.26, 99.97, and 99.47%, respectively. The exceptional removal efficiency at low concentrations can be attributed to the available active sites and the disordered and porous surface structure of biochar samples. When the Pb(II) concentration was increased to 500 mg/L, biochar samples at three different temperatures still showed high removal efficiencies of 97.92, 99.36, and 97.36%, respectively. However, the removal efficiencies at a concentration of 500 mg/L were less compared to the concentration of 50 mg/L, which is ascribed to the unavailability of more active sites to adsorb Pb ions from the solution. The results also indicate that the removal efficiency of PB550 was higher than those of PB450 and PB650, which is attributed to the more porous and available active sites present in PB550, allowing it to adsorb more Pb ions.[47]

3.2.2. Effect of Initial Pb(II) Concentration and pH. To investigate the effect of the initial concentration of Pb(II), the experiment was conducted using low concentrations ranging from 0.2 to 2 mg/L and high concentrations from 0.05 to 5 g/L of Pb(II) at ambient temperature. The pH of the metal solution influences the adsorption process. At low pH (2–4), the surface of biochar is positively charged because of the protonation of surface functional groups, suggesting the electrostatic repulsion between biochar and metal ions. The strong acidic condition of the metal solution also triggers competition between hydrogen ions and metal ions, resulting in low adsorption capacity and removal efficiency.[48] The biochar converts to a negatively charged form when the pH increases and the competition between hydrogen ions and metal ions decreases. As a

https://doi.org/10.1021/acssusresmgt.5c00556
ACS Sustain. Resour. Manage. XXXX, XXX, XXX–XXX

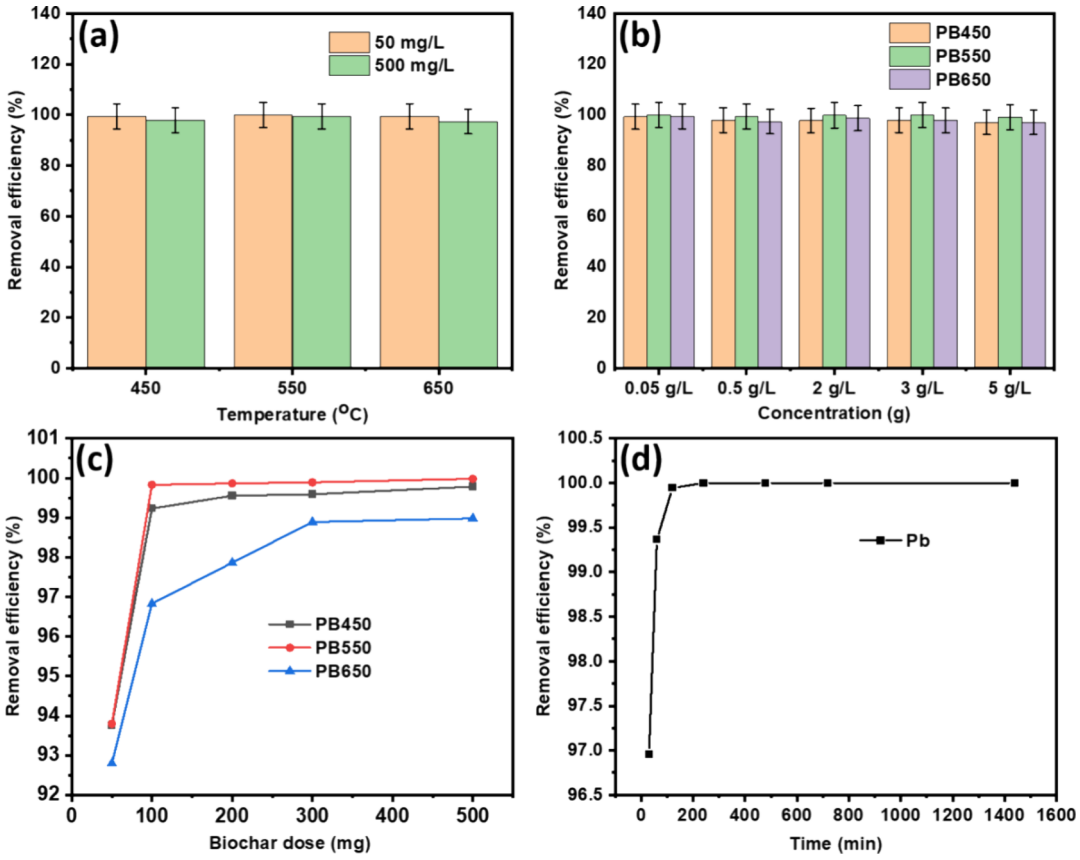

Figure 4. (a) Effect of pyrolysis temperature on removal of Pb from the Pb(II) solution using biochar produced at different temperatures; Pb(II) concentration at 50 and 500 mg/L, biochar dose = 500 mg and initial pH = 6. (b) Effect of primary concentrations of Pb(II); initial pH = 6 and biochar dose = 500 mg. (c) Effect of biochar dose prepared at different temperatures; initial pH = 6, biochar dose: 50–500 mg. (d) Effect of contact time using PB550 biochar; pH = 6, contact time: 30–1440 min, biochar dose: 500 mg.

result, biochar shows increased adsorption capacity and removal efficiency.[31] When the pH increases above 6, H^+ decreases, leading to the formation of hydroxide complexes, followed by surface precipitation, which affects the biochar's adsorption performance.[45] The adsorption efficiency was first evaluated at low concentrations, as contaminants are typically present at low levels in real-world environments. At a concentration of 0.2–2 mg/L (Figure S2), the biochar samples at three different temperatures showed outstanding removal efficiencies ranging from 98.51 to 99.99%. These indicate that biochars have numerous active sites to adsorb Pb ions at low concentrations. The Pb(II) removal efficiency decreased slowly for PB450 (from 99.26 to 97.02%) and PB650 (from 99.47 to 97.02%) with an increase in Pb(II) concentration (from 0.05 to 5 g/L). However, PB550 still shows higher removal efficiencies of 99.97, 99.96, 99.86, 99.36, and 98.98% at concentrations of 0.05, 0.5, 2.0, 3.0, and 5.0 g/L, respectively (Figure 4b). These results indicate that PB550 has abundantly active places for adsorption than PB450 and PB650. The final pH of the solution at different concentrations slightly increased to ~8.2 after adsorption, which is due to the alkaline nature of biochar.

3.2.3. Effect of Biochar Dose on Pb Removal. Figure 4c presents the effect of biochar dose on the removal of Pb. The removal efficiency increased upon increasing biochar doses from 50 to 500 mg/L for all biochar samples. The experimental results also indicate that a dosage of 500 mg/L of each biochar yields a maximum removal efficiency of Pb(II), which is attributed to the availability of more active sites in the biochar samples for removing Pb(II). The available surface area and active sites increase by increasing the biochar dosage, allowing for larger interaction between biochar and Pb(II), thereby increasing the removal efficiency.[49] Due to its distinguished surface properties, PB550 exhibited a higher adsorption efficiency (99.98%) than PB450 (99.68%) and PB650 (98.97%).

According to the above experimental findings and the adsorption study of Pb ions using biochars obtained from different temperatures, it is apparent that PB550 displayed distinct surface properties and the highest removal efficiency compared to PB450 and PB650. Therefore, only PB550 will be used to study other experiments, including adsorption kinetics and adsorption isotherms, and the results are discussed in the next sections.

3.2.4. Effect of Contact Time and Adsorption Kinetics. PB550 was used to evaluate the variations in Pb(II) removal efficiency as a function of contact time, as shown in Figure 4d. The Pb(II) ion concentration was 2 g/L (pH = 6.0), the biochar dose was 500 mg, and the contact time was 30–1440 min. As shown in Figure 4d, Pb(II) ions are quickly removed during the early stages at different contact times. This is because a large number of empty active sites are present on the surface of PB550, allowing for the effective

https://doi.org/10.1021/acssusresmgt.5c00556
ACS Sustain. Resour. Manage. XXXX, XXX, XXX–XXX

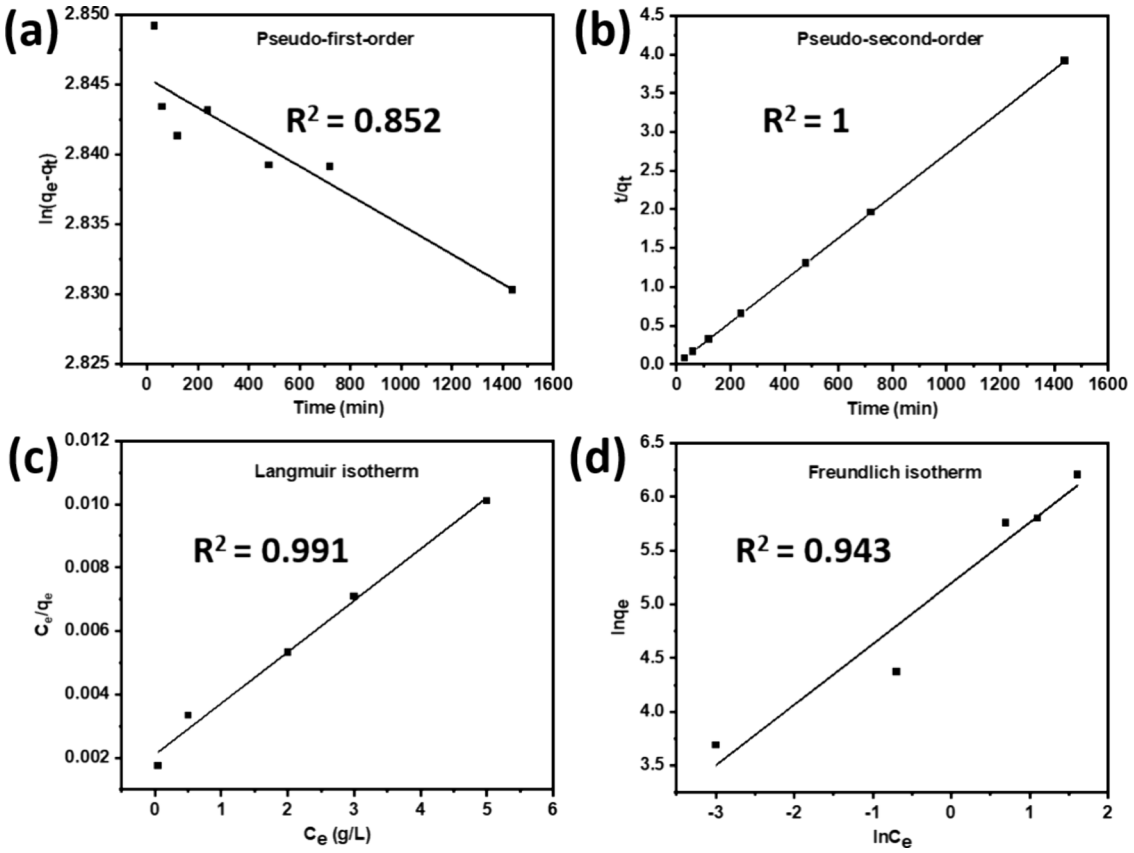

Figure 5. (a) Pseudo-first-order kinetic model, (b) pseudo-second-order kinetic model, (c) Langmuir isotherm, and (d) Freundlich isotherm for PB550 biochar.

adsorption of Pb(II) ions. Indeed, the presence of unoccupied active sites on biochar facilitates the interaction between Pb(II) ions and the active sites of biochar, which leads to the rapid removal of Pb(II) ions and then reaches a saturated condition.[50] After 120 min of contact time, the Pb(II) ion removal reached almost 100% and there were no further changes in removal efficiency at contact times of 240, 480, 720, and 1440 min.[49] To elucidate the order of reaction and rate-controlling mechanism, the kinetic analysis of Pb(II) adsorption was conducted using two popular kinetic models: pseudo-first-order (PFO) and pseudo-second-order (PSO). The kinetic adsorption of Pb(II) involves two stages, including fast adsorption and slow adsorption.

The fast adsorption occurred on the outer surface, while the slow adsorption occurred in the inner surfaces (micro and mesopores) of the adsorbent.[51] The PFO model is linked to physisorption, where the dominant forces are van der Waals interactions. On the other hand, the PSO model is associated with chemisorption, where the adsorption involves strong physicochemical interaction and electron sharing between the adsorbent and the metal ion.[52] The kinetic plots are shown in Figure 5a,b, and the kinetic parameters are presented in Table 2. Results indicated that the adsorption capacity (370.37 mg/g) and the correlation coefficient ($R^2 = 1$) of PSO are higher compared to the adsorption capacity (17.21 mg/g) and the correlation coefficient ($R^2 = 0.852$) of PFO, which implies that PSO was the most appropriate model for Pb(II) adsorption.

3.2.5. Adsorption Isotherm. The adsorption isotherms are used to illustrate the relationship between the concentration of ions and the amount of ions adsorbed per unit mass of the adsorbent at equilibrium and constant temperature.[53] The most commonly used Langmuir and Freundlich isotherm models were employed to evaluate the experimental data. The linear plots of the Langmuir and Freundlich isotherms of Pb are depicted in Figure 5c,d, and the fitting parameters are shown in Table 2. The results demonstrated that the correlation coefficient of the Langmuir isotherm model ($R^2 = 0.991$) is a better fit than the Freundlich isotherm model ($R^2 = 0.943$), indicating the homogeneous monolayer adsorption of Pb on the outer surface of PB550.[43] The calculated maximum Pb adsorption capacity (q_{max}) of 476.19 mg/g was achieved using the Langmuir isotherm model, while the Freundlich constant (K_F)/adsorption capacity was calculated by using the Freundlich model, and the calculated value was 179.47 mg/g. Evidently, the Langmuir isotherm model is more appropriate than the Freundlich model to elucidate the adsorption process of Pb.

3.2.6. Adsorption Mechanism. Adsorption is the process of mass transfer, where the metal ions are transferred from the solution to the biochar through physical and chemical interactions. Based on the properties of *Phaeodactylum* residue-derived biochar, the Pb adsorption mainly occurred through precipitation, physical adsorption, surface complexation, electrostatic interaction, hydrogen bonding, and cation exchange.[54] Figure 6 shows the possible mechanisms of Pb(II) adsorption on biochar.

https://doi.org/10.1021/acssusresmgt.5c00556
ACS Sustain. Resour. Manage. XXXX, XXX, XXX–XXX

Table 2. Pseudo-First-Order and Pseudo-Second-Order Kinetic Parameters and Fitting Parameters of Langmuir and Freundlich Isotherm Models for Adsorption of Pb(II) Ions onto *Phaeodactylum* Residue-Derived Biochar

		pseudo-first-order			pseudo-second-order		
biochar	heavy metal	q_e (mg/g)	K_1 (min^{-1})	R^2	q_e (mg/g)	K_2 (g/mg min)	R^2
PB550	Pb	17.21	0.0001	0.852	370.37	0.036	1
		Langmuir model			Freundlich model		
biochar	heavy metal	q_m (mg/g)	K_L (L/mg)	R^2	K_F (mg/g)	n	R^2
PB550	Pb	476.19	1.31	0.991	179.47	1.77	0.943

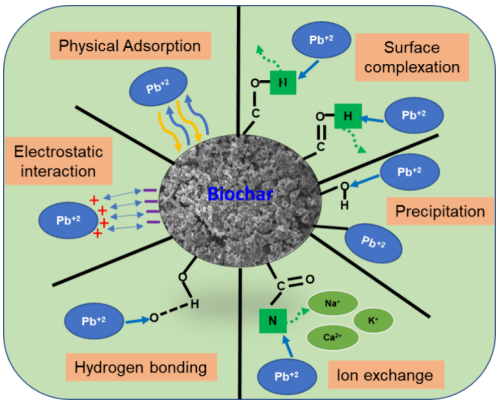

Figure 6. Adsorption mechanism of Pb by *Phaeodactylum* residue-derived biochar.

Surface precipitation is one of the important mechanisms for removing Pb from the solution. According to the XRD results, several inorganic minerals are present in the form of their salts. These are ionized in the solution as CO_3^{2-}, PO_4^{3-}, SiO_3^{2-}, and SO_4^{2-} and combined with Pb(II) ions and precipitated as $PbCO_3$, $Pb_3(PO_4)_2$, $PbSiO_3$, and $PbSO_4$.[55] The porous and disordered structure (Figure 1; SEM images) and the presence of micro- and mesopores in PB550 biochar (Figure 2; BET analysis) facilitate the penetration of Pb(II) ions into the channels and pores through physical adsorption. The adsorption of Pb(II) ions on PB550 biochar was confirmed by SEM after adsorption. Figure S3 shows the high- and low-magnification SEM images, where the structures are completely different from the SEM images before adsorption (Figure 1c,d). After adsorption, the channels and pores disappeared, demonstrating the successful adsorption of Pb(II) ions on biochar. The appearance of an obvious Pb peak in SEM-EDS analysis (Figure S5) also confirmed the adsorption and/or surface precipitation of Pb(II) ions on the biochar surface.

In order to clarify the surface complexation mechanism of the Pb(II) ion, we performed the FTIR spectra of PB550 biochar before and after adsorption, as shown in Figure S4. After adsorption, some of the peaks were missing, the peak positions at 1410 and 1045 cm^{-1} shifted to 1397 and 1033 cm^{-1}, and the sharpness of the peaks decreased. This phenomenon indicated that Pb(II) ions formed complexes with the functional groups present in PB550 biochar (Figure 3b) through coordination bonds, further confirming the effective adsorption of Pb(II) ions.[24] The hydrogen bonding occurred between Pb(II) and the hydrophilic functional groups (−OH and −COOH) on the surface of the biochar and improved the adsorption capacity.[56] Cation exchange between inorganic minerals, such as Na^+, Ca^{2+}, Mg^{2+}, K^+, and Pb(II) ions, is an important mechanism for Pb(II) adsorption. The Pb(II) ions might be exchanged with Na^+, Ca^{2+}, Mg^{2+}, and K^+, available in PB550 biochar, thereby enhancing the adsorption process.[57]

The biochar releases Na^+, K^+, Ca^{2+}, and Mg^{2+} into solution through ion exchange and dissolution. During this process, these cations are released from the biochar surface and replaced by other ions present in the surrounding water. The release of these ions increases the electrical conductivity/ionic strength of the solution, which results in the reduction of adsorption efficiency. The pH of the solution also increases due to the dissolution of alkaline ash, which significantly increases the precipitation of lead salts on the biochar surface. Secondary contamination may happen due to mineral and nutrient leaching. Large-scale use of residual algal biochar also presents potential environmental implications related to secondary contamination through mineral and nutrient leaching and the presence of intrinsic pollutants such as heavy metals and organic compounds. Reducing specific environmental risks requires careful selection of the original algal feedstock and production process, along with thorough environmental risk assessments.[58] Adsorption has emerged as a sustainable and highly efficient method for treating real industrial effluents, particularly for removing heavy metals. While laboratory studies focus on ideal conditions, validating adsorption with real wastewater requires addressing challenges like complex, multi-component mixtures, varying pH levels, and competitive adsorption.

3.2.7. Regeneration and Reuse. The recovery properties of biochar for reuse are an important factor to determine the economic feasibility of biochar. Several regeneration agents, such as HNO_3, HCl, and NaOH, were used to remove Pb(II) from biochar. In this investigation, we used HCl solution for the regeneration experiment because of its ion exchange, electrostatic repulsion, and complexation capability. The desorption efficiency of adsorbed Pb(II) typically increases with an increase in the concentration of HCl up to a certain point. An excessive amount of H^+ is produced by regeneration at a higher concentration, and this may still remain on the biochar after the desorption process. Excess H^+ ions can compete with Pb(II) ions for the available active sites on the biochar, which may reduce the adsorption efficiency of Pb(II).[59] Therefore, we selected a 0.2 M HCl solution for the regeneration of biochar.

Figure S6 presents the removal efficiency of Pb(II) for 5 consecutive adsorption–desorption cycles. The removal efficiency was 91.40% after the first biochar regeneration cycle, which is 8.7% lower than the efficiency of the initial adsorption of Pb(II). It remained stable throughout the 2nd and 3rd cycles (89.65 and 89.56%). The Pb(II) removal efficiency decreased gradually after the third cycle but remained at 82.84% by the fifth cycle, demonstrating that the PB550 biochar possesses high stability and reusability. TGA was carried out to check the

https://doi.org/10.1021/acssusresmgt.5c00556
ACS Sustain. Resour. Manage. XXXX, XXX, XXX−XXX

Table 3. Comparison of Pb Adsorption Capacities of Algae-Based Biochars

biochar type	heavy metal	adsorption capacity (mg/g)	references
Chlorella sp.	Pb	131.41	24
Gracilaria changii	Pb	36.21	53
Ulva fasciata sp.	Pb	24.15	60
Cyanidium caldarium	Pb	298.0	61
Spirulina sp.	Pb	154.56	24
Capsicum annuum L.	Pb	36.43	6
Chlorella pyrenoidosa	Pb	159.07	62
Spirulina platensis	Pb	26.9	45
Alternanthera philoxeroides	Pb	257.12	63
sugar cane bagasse	Pb	86.96	64
rice straw	Pb	253.6	65
P. tricornutum	Pb	476.19	this work

stability of PB550 after 5 consecutive adsorption–desorption cycles. As shown in Figure S7, the total weight loss of 36.7% was observed, indicating that PB550 still shows moderate stability.

The exceptional Pb(II) adsorption capacity of PB550 biochar is attributed to its notable structural properties, including the presence of micro- and mesopores, inorganic minerals, a disordered structure, active functional groups, and a moderately higher specific surface area, as confirmed by various characterization techniques. As presented in Table 3, a comparative study was made on the adsorption of Pb(II) using algal and non-algal biochars. Compared to most of the published reports on Pb(II) adsorption, *Phaeodactylum* residue-derived biochar showed a higher adsorption capacity of Pb(II).

Recently, the residual microalgae-based biochar has gained significant research interest as a sustainable alternative for different applications. However, several challenges, including consistency of quality and economic feasibility of biochar, remain significant concerns for the transition from the laboratory to industry scale. The properties of biochar, such as functional groups, surface area, stability, mineral contents, and adsorption capacity, are strongly influenced by the type of algal biomass, pyrolysis temperature, and residence time. In the laboratory scale, it is easier to control these parameters; however, slight changes in operational parameters may lead to substantial changes in biochar quality in large-scale production.[66] These critical parameters must be controlled to ensure the quality and consistency of biochar for industrial applications.

The environmental and long-term agronomic benefits of biochar are significant and diverse, resulting in increased interest in its large-scale use. Production costs, which encompass algal feedstock, pyrolysis technology, labor, transportation, and application costs, need to be optimized for large-scale implementation.[67] Lab studies play a crucial role in understanding the basic mechanisms of removal; however, applying these findings in real-world scenarios containing mixed contaminants involves complexities such as competitive adsorption, changing water chemistry, and physical aging. This tends to decrease the overall performance and predictability in comparison to results obtained in isolated laboratory settings. Additional research is needed to fill this knowledge gap and improve biochar for effective, long-term use in sustainable wastewater treatment systems.

The results of this study will inspire the utilization of residual algae biomasses in preparing biochar. In particular, the production, characterization, and application of residual algae-based biochar for wastewater treatment could be a sustainable approach in the context of the circular bioeconomy.

4. CONCLUSIONS

This work mainly focused on the utilization of residual *Phaeodactylum* residue-derived biochar as an adsorbent for Pb(II) adsorption within a circular economy context. The Pb(II) removal efficiency is significantly influenced by pyrolysis temperature, initial Pb(II) concentration, biochar dose, and contact time. The Pb(II) adsorption on PB550 biochar involved fast and slow adsorption processes. The uneven and porous nature, active functional groups, and minerals present in PB550 biochar contributed to achieving an excellent Pb(II) adsorption capacity. The Langmuir isotherm and PSO model were more suitable to describe the adsorption behavior. In conclusion, the outcomes of this investigation indicate that *Phaeodactylum* residue-derived biochar could be a promising alternative for wastewater treatment. This study also provides insight for further research on residual algae-based biochar for diverse applications.

■ ASSOCIATED CONTENT

Supporting Information

The Supporting Information is available free of charge at https://pubs.acs.org/doi/10.1021/acssusresmgt.5c00556.

SEM-EDS of biochar samples; effect of low concentration of Pb(II) on adsorption; SEM and FTIR spectra after adsorption of Pb(II); SEM-EDS of PB550 after adsorption; removal efficiency of Pb(II) for 5 adsorption–desorption cycles; and TGA curve of PB550 after 5 repeated cycles (DOCX)

■ AUTHOR INFORMATION

Corresponding Authors

Anjon Kumar Mondal – *Climate Change Cluster, University of Technology Sydney, Ultimo, NSW 2007, Australia;* orcid.org/0000-0002-0578-6984; Email: anjon.mondal@uts.edu.au

Unnikrishnan Kuzhiumparambil – *Climate Change Cluster, University of Technology Sydney, Ultimo, NSW 2007, Australia;* Email: Unnikrishnan.Kuzhiumparambil@uts.edu.au

https://doi.org/10.1021/acssusresmgt.5c00556
ACS Sustain. Resour. Manage. XXXX, XXX, XXX–XXX

Authors

Cora Hinkley – *Climate Change Cluster, University of Technology Sydney, Ultimo, NSW 2007, Australia*

C. I. Sathish – *Global Innovative Centre of Advanced Nanomaterials, School of Science, College of Engineering, Science and Environment, The University of Newcastle, Callaghan, NSW 2308, Australia*

Ajayan Vinu – *Global Innovative Centre of Advanced Nanomaterials, School of Science, College of Engineering, Science and Environment, The University of Newcastle, Callaghan, NSW 2308, Australia*; orcid.org/0000-0002-7508-251X

Stalin Kondaveeti – *Climate Change Cluster, University of Technology Sydney, Ultimo, NSW 2007, Australia*

Farjana Akter – *Climate Change Cluster, University of Technology Sydney, Ultimo, NSW 2007, Australia*

Peter Ralph – *Climate Change Cluster, University of Technology Sydney, Ultimo, NSW 2007, Australia*

Complete contact information is available at: https://pubs.acs.org/doi/10.1021/acssusresmgt.5c00556

Author Contributions

U.K.: Conceptualization, supervision, project administration, validation, review, and editing. C.H.: Data collection and analysis. C.I.S.: BET measurement, review, and editing. A.V.: Review and editing. S.K.: Data analysis, review, and editing. F.A.: Data analysis, review, and editing. P.R.: Supervision, project administration, validation, review, and editing. A.K.M.: Conceptualization, methodology, data collection and analysis, writing.

Notes

The authors declare no competing financial interest.

REFERENCES

(1) Jones, E. R.; van Vliet, M. T. H.; Qadir, M.; Bierkens, M. F. P. Country-level and gridded estimates of wastewater production, collection, treatment and reuse. *Earth Syst. Sci. Data* **2021**, *13* (2), 237–254.

(2) Koncagül, E.; Connor, R.; Abete, V. *The United Nations World Water Development Report 2024: Water for Prosperity and Peace; Facts, Figures and Action Examples*; UNESCO, **2024**.

(3) Boretti, A.; Rosa, L. Reassessing the projections of the world water development report. *npj Clean Water* **2019**, *2* (1), No. 15.

(4) Meng, X.; Hu, R. Nitrogen/phosphorus enriched biochar with enhanced porosity activated by guanidine phosphate for efficient passivation of Pb (II), Cu (II) and Cd (II). *J. Mol. Liq.* **2021**, *323*, No. 115071.

(5) Wani, A. L.; Ara, A.; Usmani, J. A. Lead toxicity: a review. *Interdiscip. Toxicol.* **2015**, *8*, 55–64.

(6) Hammo, M. M.; Akar, T.; Sayin, F.; Celik, S.; Akar, S. T. Efficacy of green waste-derived biochar for lead removal from aqueous systems: Characterization, equilibrium, kinetic and application. *J. Environ. Manage.* **2021**, *289*, No. 112490.

(7) Awual, M. R.; Hasan, M. M.; Iqbal, J.; Islam, A.; Islam, M. A.; Asiri, A. M.; Rahman, M. M. Naked-eye lead (II) capturing from contaminated water using innovative large-pore facial composite materials. *Microchem. J.* **2020**, *154*, No. 104585.

(8) World Health Organization. *Guidelines for Drinking-Water Quality: Incorporating the First and Second Addenda*; World Health Organization, **2022**.

(9) Awual, M. R. Mesoporous composite material for efficient lead (II) detection and removal from aqueous media. *J. Environ. Chem. Eng.* **2019**, *7* (3), No. 103124.

(10) Verma, A.; Kumar, S.; Kumar, S. Biosorption of lead ions from the aqueous solution by Sargassum filipendula: Equilibrium and kinetic studies. *J. Environ. Chem. Eng.* **2016**, *4* (4), 4587–4599.

(11) Xiang, W.; Zhang, X.; Chen, J.; Zou, W.; He, F.; Hu, X.; Tsang, D. C. W.; Ok, Y. S.; Gao, B. Biochar technology in wastewater treatment: A critical review. *Chemosphere* **2020**, *252*, No. 126539.

(12) Cai, Y.; Liu, L.; Tian, H.; Yang, Z.; Luo, X. Adsorption and desorption performance and mechanism of tetracycline hydrochloride by activated carbon-based adsorbents derived from sugar cane bagasse activated with ZnCl2. *Molecules* **2019**, *24* (24), 4534.

(13) Dastgerdi, Z. H.; Meshkat, S. S.; Esrafili, M. D. Enhanced adsorptive removal of Indigo carmine dye performance by functionalized carbon nanotubes based adsorbents from aqueous solution: equilibrium, kinetic, and DFT study. *J. Nanostruct. Chem.* **2019**, *9* (4), 323–334.

(14) Anastopoulos, I.; Pashalidis, I.; Hosseini-Bandegharaei, A.; Giannakoudakis, D. A.; Robalds, A.; Usman, M.; Escudero, L. B.; Zhou, Y.; Colmenares, J. C.; Núñez-Delgado, A. Agricultural biomass/waste as adsorbents for toxic metal decontamination of aqueous solutions. *J. Mol. Liq.* **2019**, *295*, No. 111684.

(15) Law, X. N.; Cheah, W. Y.; Chew, K. W.; Ibrahim, M. F.; Park, Y.-K.; Ho, S.-H.; Show, P. L. Microalgal-based biochar in wastewater remediation: Its synthesis, characterization and applications. *Environ. Res.* **2022**, *204*, No. 111966.

(16) Lucaci, A. R.; Bulgariu, D.; Popescu, M.-C.; Bulgariu, L. Adsorption of Cu (II) ions on adsorbent materials obtained from marine red algae Callithamnion corymbosum sp. *Water* **2020**, *12* (2), 372.

(17) Gupta, M.; Savla, N.; Pandit, C.; Pandit, S.; Gupta, P. K.; Pant, M.; Khilari, S.; Kumar, Y.; Agarwal, D.; Nair, R. R. Use of biomass-derived biochar in wastewater treatment and power production: A promising solution for a sustainable environment. *Sci. Total Environ.* **2022**, *825*, No. 153892.

(18) Afshar, M.; Mofatteh, S. Biochar for a sustainable future: Environmentally friendly production and diverse applications. *Results Eng.* **2024**, *23* No. 102433.

(19) Yadav, R.; Ramakrishna, W. Biochar as an environment-friendly alternative for multiple applications. *Sustainability* **2023**, *15* (18), 13421.

(20) Bayar, J.; Ali, N.; Dong, Y.; Ahmad, U.; Anjum, M. M.; Khan, G. R.; Zaib, M.; Jalal, A.; Ali, R.; Ali, L. Biochar-based adsorption for heavy metal removal in water: A sustainable and cost-effective approach. *Environ. Geochem. Health* **2024**, *46* (11), No. 428.

(21) Hu, B.; Ai, Y.; Jin, J.; Hayat, T.; Alsaedi, A.; Zhuang, L.; Wang, X. Efficient elimination of organic and inorganic pollutants by biochar and biochar-based materials. *Biochar* **2020**, *2*, 47–64.

(22) Karthik, V.; Kumar, P. S.; Vo, D.-V. N.; Sindhu, J.; Sneka, D.; Subhashini, B.; Saravanan, K.; Jeyanthi, J. Hydrothermal production of algal biochar for environmental and fertilizer applications: a review. *Environ. Chem. Lett.* **2021**, *19*, 1025–1042.

(23) Arora, N.; Tripathi, S.; Bhatnagar, P.; Guruani, P.; Philippidis, G. P.; Kumar, V.; Poluri, K. M.; Nanda, M. Algal-based biochar and hydrochar: A holistic and sustainable approach to wastewater treatment. *Chem. Eng. J.* **2024**, *496* No. 153953.

(24) Yang, Z.; Hou, J.; Wu, J.; Miao, L. The effect of carbonization temperature on the capacity and mechanisms of Pb (II) adsorption by microalgae residue-derived biochar. *Ecotoxicol. Environ. Saf.* **2021**, *225*, No. 112750.

(25) Huang, Z.; Zhang, J.; Pan, M.; Hao, Y.; Hu, R.; Xiao, W.; Li, G.; Lyu, T. Valorisation of microalgae residues after lipid extraction: Pyrolysis characteristics for biofuel production. *Biochem. Eng. J.* **2022**, *179*, No. 108330.

(26) Nguyen, D. T.; Johir, M. A. H.; Silitonga, A. S.; Salih, A. K.; Nghiem, L. D. Utilisation of spent microalgae biomass after lipid

extraction for heavy metal removal. *Environ. Sci. Pollut. Res.* **2025**, *32*, 26144 26155.
(27) Tan, X.; Zhu, S.; Show, P. L.; Qi, H.; Ho, S.-H. Sorption of ionized dyes on high-salinity microalgal residue derived biochar: Electron acceptor-donor and metal-organic bridging mechanisms. *J. Hazard. Mater.* **2020**, *393*, No. 122435.
(28) Costa, J. A. V.; Zaparoli, M.; Cassuriaga, A. P. A.; Cardias, B. B.; da Silva Vaz, B.; de Morais, M. G.; Moreira, J. B. Biochar production from microalgae: a new sustainable approach to wastewater treatment based on a circular economy. *Enzyme Microb. Technol.* **2023**, *169*, No. 110281.
(29) Jaiswal, K. K.; Kumar, V.; Vlaskin, M. S.; Nanda, M.; Verma, M.; Ahmad, W.; Kim, H. Hydropyrolysis of freshwater macroalgal bloom for bio-oil and biochar production: kinetics and isotherm for removal of multiple heavy metals. *Environ. Technol. Innovation* **2021**, *22*, No. 101440.
(30) Verma, M.; Kumar, A.; Singh, K. P.; Kumar, R.; Kumar, V.; Srivastava, C. M.; Rawat, V.; Rao, G.; Kumari, S.; Sharma, P. Graphene oxide-manganese ferrite (GO-MnFe2O4) nanocomposite: One-pot hydrothermal synthesis and its use for adsorptive removal of Pb2+ ions from aqueous medium. *J. Mol. Liq.* **2020**, *315*, No. 113769.
(31) Jaiswal, K. K.; Kumar, V.; Verma, R.; Verma, M.; Kumar, A.; Vlaskin, M. S.; Nanda, M.; Kim, H. Graphitic bio-char and bio-oil synthesis via hydrothermal carbonization-co-liquefaction of microalgae biomass (oiled/de-oiled) and multiple heavy metals remediations. *J. Hazard. Mater.* **2021**, *409*, No. 124987.
(32) Mondal, A. K.; Hinkley, C.; Kondaveeti, S.; Vo, P. H. N.; Ralph, P.; Kuzhiumparambil, U. Influence of pyrolysis time on removal of heavy metals using biochar derived from macroalgal biomass (Oedogonium sp.). *Bioresour. Technol.* **2024**, *414*, No. 131562.
(33) Shaikh, W. A.; Chakraborty, S.; Islam, R. U.; Ghfar, A. A.; Naushad, M.; Bundschuh, J.; Maity, J. P.; Mondal, N. K. Fabrication of biochar-based hybrid Ag nanocomposite from algal biomass waste for toxic dye-laden wastewater treatment. *Chemosphere* **2022**, *289*, No. 133243.
(34) Arif, M.; Li, Y.; El-Dalatony, M. M.; Zhang, C.; Li, X.; Salama, E.-S. A complete characterization of microalgal biomass through FTIR/TGA/CHNS analysis: An approach for biofuel generation and nutrients removal. *Renewable Energy* **2021**, *163*, 1973–1982.
(35) Singh, S.; Singh, A.; Singh, S.; Prasad, N.; Singh, P.; Asthana, R. K. IAA induced biomass and lipid overproduction in microalga via two-stage cultivation strategy: Characterization using FTIR/CHNS/TGA/DTG and 1H-NMR for bioenergy potential. *Energy Convers. Manage.* **2024**, *311*, No. 118546.
(36) Koçer, A. T.; Özçimen, D. Determination of combustion characteristics and kinetic parameters of Ulva lactuca and its biochar. *Biomass Convers. Biorefin.* **2021**, *14* 5913–5922.
(37) Mondal, A. K.; Hinkley, C.; Krishnan, L.; Ravi, N.; Akter, F.; Ralph, P.; Kuzhiumparambil, U. Macroalgae-based biochar: preparation and characterization of physicochemical properties for potential applications. *RSC Sustainability* **2024**, *2*, 1828.
(38) Anand, A.; Gautam, S.; Ram, L. C. Feedstock and pyrolysis conditions affect suitability of biochar for various sustainable energy and environmental applications. *J. Anal. Appl. Pyrolysis* **2023**, *170*, No. 105881.
(39) Sanka, P. M.; Rwiza, M. J.; Mtei, K. M. Removal of selected heavy metal ions from industrial wastewater using rice and corn husk biochar. *Water, Air, Soil Pollut.* **2020**, *231*, 244.
(40) Choi, Y.-K.; Choi, T.-R.; Gurav, R.; Bhatia, S. K.; Park, Y.-L.; Kim, H. J.; Kan, E.; Yang, Y.-H. Adsorption behavior of tetracycline onto Spirulina sp. (microalgae)-derived biochars produced at different temperatures. *Sci. Total Environ.* **2020**, *710*, No. 136282.
(41) Sahoo, S. S.; Vijay, V. K.; Chandra, R.; Kumar, H. Production and characterization of biochar produced from slow pyrolysis of pigeon pea stalk and bamboo. *Cleaner Eng. Technol.* **2021**, *3*, No. 100101.
(42) Chen, Y.-d.; Lin, Y.-C.; Ho, S.-H.; Zhou, Y.; Ren, N.-q. Highly efficient adsorption of dyes by biochar derived from pigments-extracted macroalgae pyrolyzed at different temperature. *Bioresour. Technol.* **2018**, *259*, 104–110.
(43) Yang, W.; Wang, Z.; Song, S.; Han, J.; Chen, H.; Wang, X.; Sun, R.; Cheng, J. Adsorption of copper (II) and lead (II) from seawater using hydrothermal biochar derived from Enteromorpha. *Mar. Pollut. Bull.* **2019**, *149*, No. 110586.
(44) Tan, X.; Wang, H.; Guo, X.; Ho, S.-H. Effects of nitrogen doped-biochar on wastewater remediation. *Environ. Technol. Innovation* **2023**, *32*, No. 103413.
(45) Myung, E.; Kim, H.; Choi, N.; Cho, K. The biochar derived from Spirulina platensis for the adsorption of Pb and Zn and enhancing the soil physicochemical properties. *Chemosphere* **2024**, *364*, No. 143203.
(46) Shang, S.; Che, W.; Li, Y. Removal of Cr (VI) from water using microalgae-based modified biochar: Adsorption performance, mechanisms, and life cycle assessment. *Algal Res.* **2025**, *85*, No. 103819.
(47) Maiti, P.; Meikap, B. C. Mechanism and adsorptive removal of Pb (II) by torrefied/pyrolyzed functionalized bio-adsorbent in batch application and life cycle assessment. *Sep. Purif. Technol.* **2025**, *354*, No. 129333.
(48) Liu, W.; Li, K.; Hu, X.; Hu, X.; Zhang, R.; Li, Q. Characteristics and mechanism of Pb2+ adsorption from aqueous solution onto biochar derived from microalgae and chitosan-modified microalgae. *Front. Environ. Chem.* **2021**, *2*, No. 693509.
(49) Ravindiran, G.; Rajamanickam, S.; Ramalingam, M.; Hayder, G.; Sathaiah, B. K.; Gaddam, M. K. R.; Muniasamy, S. K.; Arunkumar, P. Conversion of seaweed waste to biochar for the removal of heavy metal ions from aqueous solution: A sustainable method to address eutrophication problem in water bodies. *Environ. Res.* **2024**, *241*, No. 117551.
(50) Olawale, S. A.; Bonilla-Petriciolet, A.; Mendoza-Castillo, D. I.; Okafor, C. C.; Sellaoui, L.; Badawi, M. Thermodynamics and mechanism of the adsorption of heavy metal ions on keratin biomasses for wastewater detoxification. *Adsorpt. Sci. Technol.* **2022**, *2022*, No. 7384924.
(51) Liu, P.; Rao, D.; Zou, L.; Teng, Y.; Yu, H. Capacity and potential mechanisms of Cd (II) adsorption from aqueous solution by blue algae-derived biochars. *Sci. Total Environ.* **2021**, *767*, No. 145447.
(52) Mostafapour, F. K.; Mahvi, A. H.; Khatibi, A. D.; Saloot, M. K.; Mohammadzadeh, N.; Balarak, D. Adsorption of lead (II) using bioadsorbent prepared from immobilized Gracilaria corticata algae: thermodynamics, kinetics and isotherm analysis. *Desalin. Water Treat.* **2022**, *265*, 103–113.
(53) Isam, M.; Baloo, L.; Chabuk, A.; Majdi, A.; Al-Ansari, N. Optimization and modelling of Pb (II) and Cu (II) adsorption onto red algae (Gracilaria changii)-based activated carbon by using response surface methodology. *Biomass Convers. Biorefin.* **2024**, *14* (15), 16799–16818.
(54) Li, H.; Dong, X.; da Silva, E. B.; de Oliveira, L. M.; Chen, Y.; Ma, L. Q. Mechanisms of metal sorption by biochars: Biochar characteristics and modifications. *Chemosphere* **2017**, *178*, 466–478.
(55) Wang, Z.; Liu, G.; Zheng, H.; Li, F.; Ngo, H. H.; Guo, W.; Liu, C.; Chen, L.; Xing, B. Investigating the mechanisms of biochar's removal of lead from solution. *Bioresour. Technol.* **2015**, *177*, 308–317.
(56) Jiang, F.; Li, F.; Zimmerman, A. R.; Yu, Z.; Ji, L.; Wei, C.; Zhang, X.; Gao, B. Remarkable synergy between sawdust biochar and attapulgite/diatomite after co-ball milling to adsorb methylene blue. *RSC Adv.* **2023**, *13* (21), 14384–14392.
(57) Zhang, J.; Ma, X.; Yuan, L.; Zhou, D. Comparison of adsorption behavior studies of Cd2+ by vermicompost biochar and KMnO4-modified vermicompost biochar. *J. Environ. Manage.* **2020**, *256*, No. 109959.
(58) Dong, M.; Jiang, M.; He, L.; Zhang, Z.; Gustave, W.; Vithanage, M.; Niazi, N. K.; Chen, B.; Zhang, X.; Wang, H. Challenges in safe environmental applications of biochar: Identifying risks and unintended consequence. *Biochar* **2025**, *7* (1), 12.
(59) Do, X.-H.; Lee, B.-K. Removal of Pb^{2+} using a biochar−alginate capsule in aqueous solution and capsule regeneration. *J. Environ. Manage.* **2013**, *131*, 375–382.

https://doi.org/10.1021/acssusresmgt.5c00556
ACS Sustain. Resour. Manage. XXXX, XXX, XXX–XXX

(60) Suresh Jeyakumar, R. P.; Chandrasekaran, V. Adsorption of lead (II) ions by activated carbons prepared from marine green algae: equilibrium and kinetics studies. *Int. J. Ind. Chem.* **2014**, *5*, 10.
(61) Cho, Y.-L.; Lee, Y.-C.; Hsu, L.-C.; Wang, C.-C.; Chen, P.-C.; Liu, S.-L.; Teah, H.-Y.; Liu, Y.-T.; Tzou, Y.-M. Molecular mechanisms for Pb removal by Cyanidiales: a potential biomaterial applied in thermo-acidic conditions. *Chem. Eng. J.* **2020**, *401*, No. 125828.
(62) Rohman, G. A. N.; Aziz, M. A.; Nawaz, A.; Elgzoly, M. A.; Hossain, M. M.; Razzak, S. A. High-performance biochar from Chlorella pyrenoidosa algal biomass for heavy metals removal in wastewater. *Sep. Purif. Technol.* **2024**, *341*, No. 126870.
(63) Yang, Y.; Wei, Z.; Zhang, X.; Chen, X.; Yue, D.; Yin, Q.; Xiao, L.; Yang, L. Biochar from Alternanthera philoxeroides could remove Pb (II) efficiently. *Bioresour. Technol.* **2014**, *171*, 227–232.
(64) Abdelhafez, A. A.; Li, J. Removal of Pb (II) from aqueous solution by using biochars derived from sugar cane bagasse and orange peel. *J. Taiwan Inst. Chem. Eng.* **2016**, *61*, 367–375.
(65) Deng, J.; Li, X.; Liu, Y.; Zeng, G.; Liang, J.; Song, B.; Wei, X. Alginate-modified biochar derived from Ca (II)-impregnated biomass: Excellent anti-interference ability for Pb (II) removal. *Ecotoxicol. Environ. Saf.* **2018**, *165*, 211–218.
(66) Santos, D. C. B. D.; Evaristo, R. B. W.; Dutra, R. C.; Suarez, P. A. Z.; Silveira, E. A.; Ghesti, G. F. Advancing biochar applications: a review of production processes, analytical methods, decision criteria, and pathways for scalability and certification. *Sustainability* **2025**, *17* (6), 2685.
(67) Campion, L.; Bekchanova, M.; Malina, R.; Kuppens, T. The costs and benefits of biochar production and use: A systematic review. *J. Cleaner Prod.* **2023**, *408*, No. 137138.

https://doi.org/10.1021/acssusresmgt.5c00556
ACS Sustain. Resour. Manage. XXXX, XXX, XXX–XXX